Optical and Quantum Electronics (2024) 56:178
https://doi.org/10.1007/s11082-023-05753-1

Influence of Eu^{3+} ions on physical, mechanical and radiation shielding properties of B_2O_3–CaO–Bi_2O_3 glasses: Experimental and simulation investigation

Norah A. M. Alsaif[1] · Haifa I. Alrebdi[1] · Y. S. Rammah[2] · R. A. Elsad[3] · E. M. Mounir[1]

Received: 21 September 2023 / Accepted: 6 November 2023 / Published online: 14 December 2023

Abstract
High density glass samples of chemical composition $70B_2O_3$–20CaO–(10 − x) Bi_2O_3–xEu_2O_3: 0 (BCBEu0.0) ≤ x ≤ 1 (BCBEu1.0) mol% were synthesized by melt-quenched route. The amorphous structure of glass blocks is established by the X-ray diffraction (XRD) spectrum. The physical, mechanical properties as well as gamma-ray shielding characteristics of the synthesized glass blocks were investigated. Density of samples showed an increment from 5.0373 to 5.0736 gcm^{-3}. The molar volume decreased from 25.012 cm^3/mol for BCBEu0.0 (Eu = 0.0) to 24.605cm^3/mol for BCBEu1.0 (Eu = 1.0). Elastic moduli and Poisson's ratio have been estimated according to Makishima and Mackenzie via the system values of dissociation free energies and packing densities. The oxygen molar volume decreased from 9.62 to 9.46346 cm^3/mol, whereas Poisson's glasses ratio varies between 0.250 and 0.257 as the [Eu_2O_3] mol% is improved from 0 to 1.0 mol%. Young's modulus has a value of 63.202 GPa and increased to 65.002 GPa at lower and higher [Er_2O_3] mol%, respectively. Shielding properties of investigated glasses have been estimated utilizing XCOM, and Phys-X/PSD program. Mass and linear attenuation coefficient were found to increase as the mol% of Eu_2O_3 increased. The sample coded as BCBEu1.0 with high density possessed lowest values of half-value layer. The glass BCBEu1.0 pointed out to be a superior when used as radiation protection agent. The suggested glass sample loaded with high concentration of europium has a strong ability to guard against radiation as compared to glasses without and low concentration of europium and it can be used in the field of medicine, according to the results.

Keywords Density · Mechanical properties · Molar volume · Phy-X · MAC · Half-value layer · Melt-quenching route

1 Introduction

Rare-earth (RE) elements-doped glass systems have gained popularity for a diverse array of uses, such as solid-state-laser, emission displays, optical-amplifiers, and converting IR to UV light (Khan et al. 2019; Adam 2002). The rationale behind it lies in the exceptional attributes of these glass types: their transparency, substantial amplification, proficient

Extended author information available on the last page of the article

handling of temperature-induced optical changes, and their resistance to chemical processes. Moreover, compared to their single crystal counterparts, bulk-glasses infused with RE-elements were conveniently manufactured in desired forms and flexibility (Khan et al. 2019; Babu et al. 2007; Lavın et al. 2003). Furthermore, this production process is both efficient and cost-effective, ensuring consistent optical uniformity and the potential for distinct luminescence features across a broader spectrum. A former oxide glass variant, known as B_2O_3, employs flat BO3 units as its foundational structure. The incorporation of modifier oxide glasses like Li_2O, ZnO, and CaO can transmute these planar BO3 units into tetrahedral BO4 units (Lavın et al. 2003; Bray 1999; Michaelis et al. 2007; Yiannopoulos et al. 2001; Sallam et al. 2020; Abdel Maksoud et al. 2022; Madbouly et al. 2022). Glasses composed of borate, particularly B_2O_3, showcase remarkable physical and chemical traits, resilience to high temperatures, and spectral light transmission across the range from near UV to IR. Given these attributes, B_2O_3 glass stands as a propitious matrix of embedding RE-metal ions, especially pertinent for a variety of optoelectronic applications (Lavın et al. 2003; Madbouly et al. 2022).

In relation to the matrix in which they are embedded, Europium (Eu^{2+} and Eu^{3+}) ions tend to absorb light photons within UV spectrum and showcase emission spectra spanning from the UV to regions close to the infrared (IR) (Khan et al. 2019; Babu et al. 2007; Niraula and Rizal 2018; Poort et al. 1996; El-Denglawey et al. 2021; Alsaif et al. 2022a, 2022b; Rammah et al. 2021a; Hegde et al. 2022). The alteration in electron positioning between the $_4F^7$ fundamental state and the crystal field portion of the $_4F^6 \rightarrow {}_5D^7$ excited state configuration gives rise to the crimson luminescence of Eu^{3+} ions, diverging from the verdant luminescence exhibited by Eu^{2+} ions (Poort et al. 1996). Consequently, the arrangement and nature of the chemical bonds within the glass framework have a direct impact on the optical traits of RE ions (Lavın et al. 2003; Madbouly et al. 2022).

Upon the inclusion of PbO and/or Bi_2O_3 alongside Eu_2O_3 within the glass compositions, a discernible enhancement in their capacity to mitigate radiation has been ascertained (Hegde et al. 2022; Wagh et al. 2017; Rammah et al. 2021b, 2020). The examination and manipulate of Eu^{3+} ions in the glass compositions on shielding-mitigating traits of diverse glass types has been undertaken by researchers such as Wagh et al. (2017), Rammah et al. (2021b), and Hegde et al. (2022). Their collective findings concur that the introduction of Eu^{3+} ions into glass formulations can effectively heighten their proficiency in mitigating radiation effects.

In this research work, novel bismuth borate glass systems that contain the europium (Eu^{3+}) rare earth ions are prepared. These glasses were created using the traditional melting process. The prepared glasses' structure, physical (e.g., density, and oxygen packing density), mechanical, and effectiveness against harmful radiations were tested for medical applications.

2 Experimental work

2.1 Glass-blocks preparations

The produced glasses were coded as:

BCBEu0.0: $70B_2O_3$–20CaO–$10Bi_2O_3$–$0.0Eu_2O_3$,
BCBEu0.2: $70B_2O_3$–20CaO–$9.8Bi_2O_3$–$0.2Eu_2O_3$,

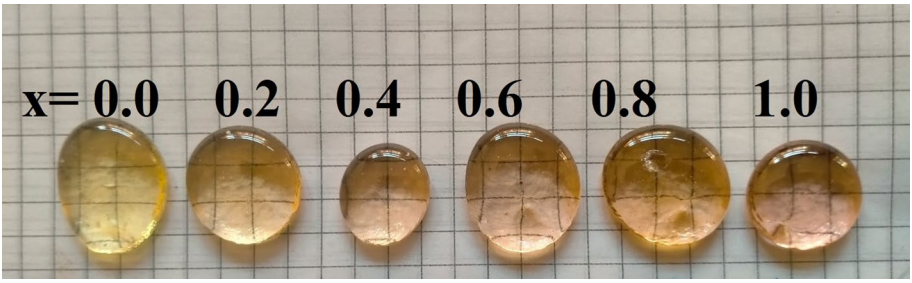

Fig. 1 A photo of the prepared glass samples (x = 0.0, 0.2, 0.4, 0.6, 0.8, and 1.0 mol%)

Table 1 Composition, density, and molar volume for prepared glass samples of $70B_2O_3{\cdot}20CaO{\cdot}(10-x)Bi_2O_3{\cdot}xEu_2O_3$, $0 \le x \le 1$ mol% glasses

Samples code	Chemical compositions mol%				Density, ρ_{glass} (g/cm^3) ± 0.001	Molar volume, V_m (cm^3/mol) ± 0.001
	B_2O_3	CaO	Bi_2O_3	Eu_2O_3		
BCBEu0.0	70	20	10	0.0	5.037	25.012
BCBEu0.2	70	20	9.8	0.2	5.044	24.931
BCBEu0.4	70	20	9.6	0.4	5.052	24.843
BCBEu0.6	70	20	9.4	0.6	5.059	24.760
BCBEu0.8	70	20	9.2	0.8	5.066	24.681
BCBEu1.0	70	20	9	1.0	5.074	24.605

BCBEu0.4: $70B_2O_3$–20CaO–$9.6Bi_2O_3$–$0.4Eu_2O_3$,
BCBEu0.6: $70B_2O_3$–20CaO–$9.4Bi_2O_3$–$0.6Eu_2O_3$,
BCBEu0.8: $70B_2O_3$–20CaO–$9.2Bi_2O_3$–$0.8Eu_2O_3$, and
BCBEu1.0: $70B_2O_3$–20CaO–$9Bi_2O_3$–$1.0Eu_2O_3$,

The general chemical compositions of the prepared samples was $70B_2O_3$–20CaO–$(10–x)Bi_2O_3$–xEu_2O_3: $0 \le x \le 1$ mol%. Samples were set by traditional melt-quenched method. B_2O_3, CaO, Bi_2O_3, and Eu_2O_3 oxides with purity 99% were used in preparation process. The total weight of each mixture composite was 10 g. Firstly, powders were precisely weighed in accordance with the mol% and thoroughly mixed in a mortar for 30 min to guarantee good homogeneity. The resultant mixture was then put in uncovered 50 mL porcelain crucibles and cooked for 45 min at 300 °C in a regular environment in an electric oven. Then it was transferred to another electric oven and heated to 1200 °C for 30 min to create a clear-highly-viscous liquid. Before being quenched into a stainless-steel mold, a viscous glass solution was intermittently spun for 10 min in an electric furnace to achieve homogeneity. The finished glass disks were then heated to 300 °C for a day to remove any thermal stresses and forming bubbles. Photographic pictures of the prepared glass blocks are depicted in Fig. 1. Samples codes and chemical composition of the prepared blocks are shown in Table 1.

2.2 XRD measurement

After the fabrication process, the little pieces were ground to provide some powders for this characterisation step. Using a German Bruker AXS D8 Advance X-ray diffractometer, the XRD diffraction study of glasses loaded with different contents of europium was performed within the values of 2θ between 10° and 80°. An analysis was conducted using CuK radiation.

2.3 Measurements of density and other associated parameters

Through the application of Archimedes' principle and immersion in toluene, the density of produced glass samples was determined at room temperature using the following relationship:

$$\rho = \left(\frac{W_{air}}{W_{air} - W_{Toluene}} \right) \times \rho_{Toluene} \tag{1}$$

where W_{air} and $W_{Toluene}$ represent its mass in air and after being submerged in toluene, respectively.

Equation (2) is used to determine the glass's molar volume (V_m).

$$V_m = \frac{Molecular\ weight\ of\ glass\ sample}{\rho_{glass}} \tag{2}$$

Oxygen packing density (OPD) gives information about the tightness of glass network and is determined according the following formula (Divina et al. 2020):

$$OPD = 1000\ N \frac{\rho_{glass}}{Molecular\ weight\ of\ glass\ sample} \tag{3}$$

where N is total number of oxygen atoms.

The following formula (Divina et al. 2020) is used to compute the oxygen molar volume (OMV), or the volume of glass that contains one mol of oxygen.

$$OMV = \frac{V_m}{\sum x_i n_i} \tag{4}$$

where n_i is the number of oxygen atoms in each component oxide and x_i is the molar percentage of each constituent.

2.4 The elastic–mechanical properties

To investigate the mechanical features of the glasses specimen under inspection, the Makishima–Mackenzie hypothesis (Makishima and Mackenzie 1975) was utilized in this investigation.

2.5 Photon shielding competences

The Phys-X/PSD program was used to evaluate radiation shielding parameters (Rammah et al. 2021b).

3 Results and discussion

3.1 XRD patterns

Figure 2 illustrates the XRD of prepared BCBEu-glasses. For all patterns, the distinctive diffraction peaks were identified very sharpens at about 29°. In addition, it is possible to see hump in all XRD footprint of glass samples and the absence of prominent diffraction peaks. These observations demonstrate that all prepared glasses are amorphous.

3.2 Physical characteristics

The measured density and calculated theoretical molar volume of the specimens have been detailed in Table 1 and Fig. 3. The variations in sample densities emerged in relation to the addition of europium(III) oxide (Eu_2O_3) to the chemical composition of the obtained blocks. The density progressed from 5.0373 to 5.0736 g/cm^3 as the Eu_2O_3 mol% rose from 0.0 to 1.0 mol% within glasses. However the density of bismuth is higher than the density of europium, the replacement of bismuth with europium in the current study enhances the density. The inclusion of europium ions may skew the scale of the rising synthesis of tetrahedral BO4 units at the expense of triangles BO3. Tetrahedral BO4 groups that are connected in three dimensions have a significantly higher density than planar BO3 triangles (Elsad et al. 2021a; Khattari et al. 2022). The density of BO_{CN} increases from 1867 to 3110 kgm^{-3} when the coordination number (CN) is increased from 3 to 4 (Elsad et al. 2021a). The rising trend of glass system density is thus explained by the increasing production of denser tetrahedral BO4 units at the decrease of less dense BO3 triangles.

Figure 3 also indicates that the molar volume (V_m) and density exhibit the opposite trend. Furthermore, we ascertained that $V_m \in [25.012, 24.605]$ cm^3/mol with the introduction of europium(III) oxide to the glass's chemical composition. The change in glass structure caused by variations in the concentration of BO3 and BO4 units may also be connected to the molar volume decreasing with an increase in europium content. Rapid BO4 tetrahedral formation is a significant factor in the reduction of molar volume. The molar volumes of triangle BO3 and tetrahedral BO4 units are 37.4 and 22.4 cm^3 mol^{-1},

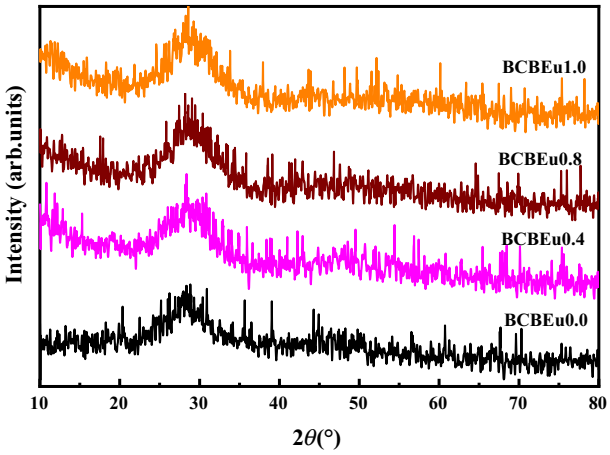

Fig. 2 XRD patterns of the synthesized glasses

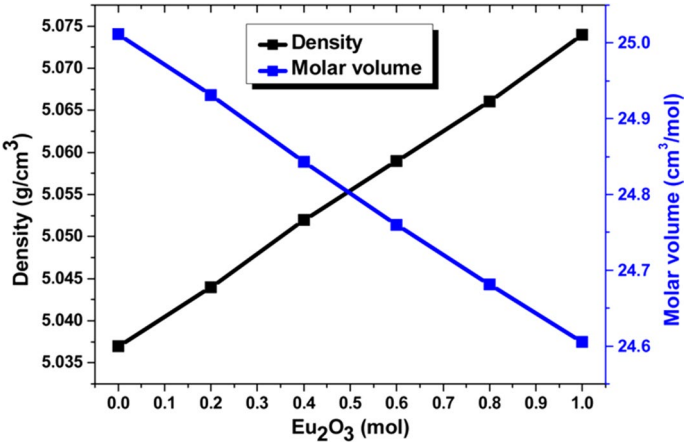

Fig. 3 Variation of density and molar volume as a function of Eu_2O_3 molar fraction present in glass samples

respectively, which are significantly different (Elsad et al. 2021a). Such formed massive BO4 units explain clearly closing the glass structure.

Figure 4 depicts an increase in oxygen packing density (OPD) that runs counter to the trend seen in oxygen molar volume (OMV). Notably, in such unique glass structures, OMV decreased from 9.62 cm^3/mol at $[Eu_2O_3] = 0$ mol% to 9.46346 cm^3/mol at $[Eu_2O_3] = 1.0$ mol%. In contrast, OPD escalated from 103.96 to 105.66 g atom/L, marking a fractional change of 1.63%. Such alteration signifies that the inclusion of europium (III) oxide in the glass specimens has effects on both OPD and OMV. For the present glass matrix, the enhancement in OPD and reduction in OMV with the increasing content of Eu_2O_3 confirm the more packed structure of glass matrix due to the presence of more bridging oxygens (BOs) in the structure.

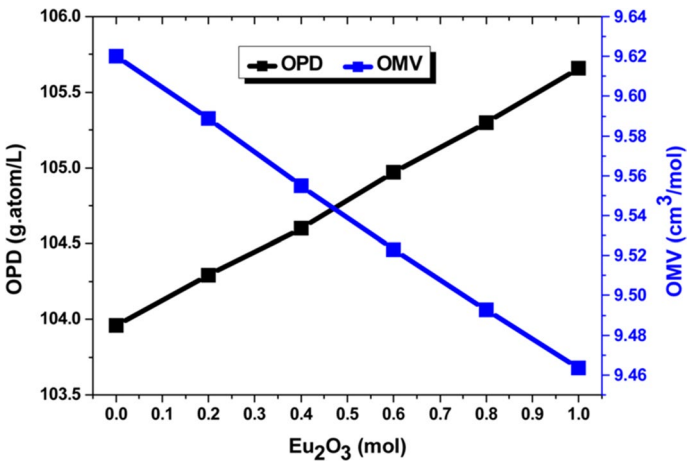

Fig. 4 Oxygen molar volume (OMV) and oxygen packing density (OPD) as a function of E Eu_2O_3 molar fraction presented in glass samples

3.3 The elastic–mechanical properties

In this investigation, the Makishima–Mackenzie theory (Makishima and Mackenzie 1975) was employed to explore the mechanical-characteristics of glasses specimen under examination. The summarized outcomes for estimated elastic-moduli and the Poisson's-ratio are conveniently presented in Table 2. The findings reveal that the Poisson's ratio for the glass range shifts within 0.250–0.257 as the molar proportion of [Eu_2O_3] escalates from 0 to 1.0 mol%. The thermo-dynamical attributes of the glasses structure embedded in the Gibbs-free energies (G) are also made accessible through Table 2. This parameter commences at 56.66 kJ/cm^3 at lower [Eu_2O_3] mol% and advances to 56.78 kJ/cm^3 as the concentration of Eu_2O_3 intensifies in the glassy framework. The associated dissociation free energy (G_t) for the entire glass system increases as a result of raising boron's coordination from 3 to 4.

Moreover, additional moduli displayed an augmentation as the molar content of [Eu_2O_3] within the molecular configuration of the glassy structure increased. As an illustration, Young's modulus, initially at 63.202 GPa, exhibited an elevation to 65.002 GPa for lower and higher [Eu_2O_3] concentrations. Also recorded shear modulus and bulk modulus in Table 2 are notably enhanced with increasing Eu_2O_3 concentration. The interrelation of elastic–physical characteristics in such glass compositions was influenced by the bonding forces between atoms, the extent of atomic arrangement, and the unit cell's spatial orientation factor (To et al. 2020). The increasing dimensionality and interconnection of networks are primarily responsible for this evident enhancement in elastic moduli. As was previously mentioned, the addition of Eu_2O_3 causes a rising amount of higher coordination [BO4] over lower coordination [BO3]. Accurate determination of these structural attributes remains challenging due to inherent limitations in experimental methodologies. Consequently, incorporating bonds dissociations energies and V_m of the used oxides into numerical computations might introduce disparities between anticipated and observed behaviors within the studied glass compositions.

3.4 Gamma-ray shielding properties

Figure 5a presents a three-dimensional logarithmic representation illustrating the computed MAC values acquired from two methods (XCOM (Berger et al. xxxx) and Phys-X (Şakar et al. 2020)) in the energies spanning $E \in [0.015–15]$ MeV. MAC trend with

Table 2 The mechanical parameters and elastic moduli of the investigated samples

Sample code	V_t (cm^3/mol) packing densities	G Dissociation energies (kJ/cm^3)	E Young modulus (GPa)	B Bulk modulus (GPa)	S Shear modulus (GPa)	Σ Poisson's ratio
BCBEu0.0	0.557	56.66	63.202	42.299	25.261	0.250
BCBEu0.2	0.560	56.68	63.556	42.756	25.376	0.252
BCBEu0.4	0.564	56.70	63.930	43.242	25.498	0.253
BCBEu0.6	0.567	56.73	64.295	43.719	25.617	0.254
BCBEu0.8	0.570	56.76	64.651	44.184	25.734	0.256
BCBEu1.0	0.572	56.78	65.002	44.645	25.849	0.257

respect to incoming photon energy aligns well with an exponential decay function (Elsad et al. 2021b). Additionally, the average inferred discrepancy between these two techniques remains below 6%. photoelectric absorption (PE), Compton scattering (CS), and pair production (PP) are the three predicted interactions that can occur at low, middle, and high energies, respectively, depending on the energy of the input photon. Due to the dominating PE absorption, which has a high effective cross section correlated with the incident energy and absorber atomic number ($1/E^{3.5}$ and Z^4), the absorber will consequently exhibit high MAC values (Divina et al. 2020).

For instance, at E = 15.0 keV, the computed MAC values are 40.627, 40.773, 40.919, 41.064, 41.207, and 41.350 cm^2/g for the BCBEu0.0, BCBEu0.2, BCBEu0.4, BCBEu0.6, BCBEu0.8, and BCBEu1.0 samples, respectively. These values correspond to a percentage increase of 0.723 cm^2/g between the lower and higher concentrations of Eu_2O_3 in the blocks. This trend is expected due to the minor variation (1.0 mol%) of europium (III) oxide in the samples. The increasing MAC as a function of molar concentration of Eu_2O_3 or the sample densities increases is evident. This behavior is consistent even at higher-energy incoming photons, where these values tend to converge.

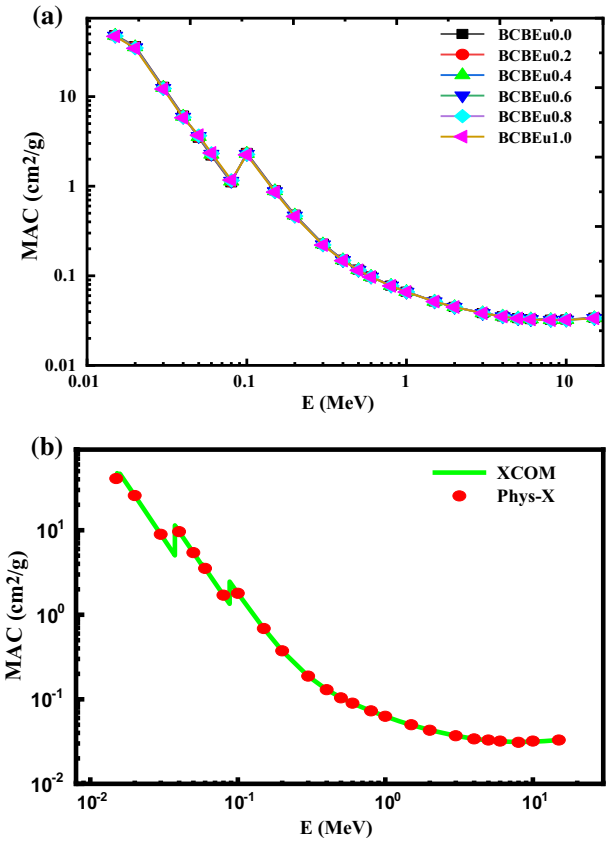

Fig. 5 **a** The MAC calculated using Phys-X for the studied samples; **b** a comparison of the MAC values between XCOM data base Phys-X program for the sample encoded as BCBEu0.4

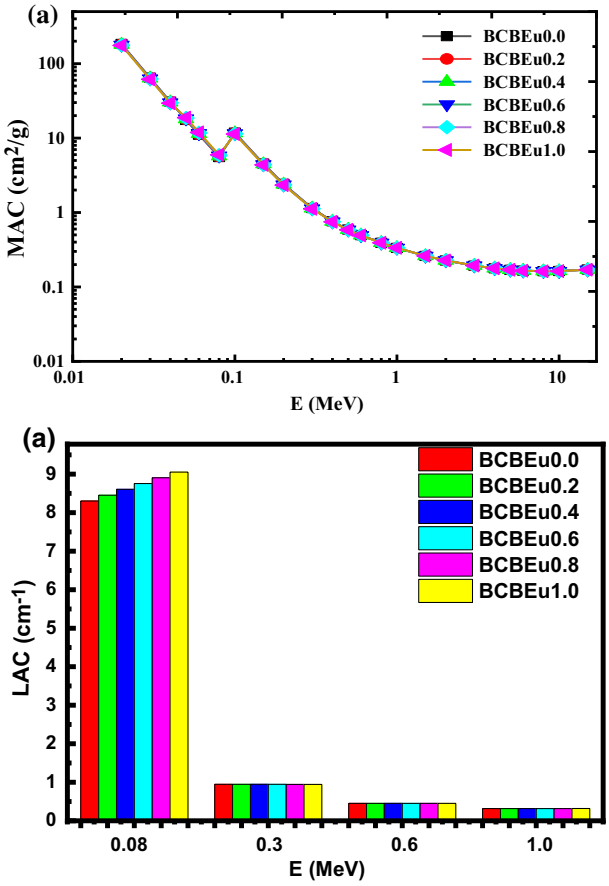

Fig. 6 **a** A comparative 3D illustration of the LAC as function incoming photon energy. **b** A comparison of the LAC values at selected incoming photon energies

For instance, the ratio of MAC at E = 5 MeV to that at E = 15 MeV remains around 1.00%, regardless of the sample's properties or Eu_2O_3 content.

This ratio emphasizes the intertwined influence of Molarity and photon energies on this crucial shielding-radiation factor. A similar reliance on mol% was also observed in the studied physico-mechanics of these solids as discussed earlier. This substantiates that the molar fraction of [Eu_2O_3] significantly influences the physical, mechanical, and shielding characteristics of the studied glass systems. Furthermore, with increasing incoming photon energy, MAC values decrease notably faster compared to lower energy levels. For E = 0.015 MeV, the MAC values ranged from 40.627 to 41.350 cm^2/g as the [Eu_2O_3] concentration increases from 0 to 1.0 mol%. Moreover, at E = 15 MeV, these values remain nearly constant (around 0.033 cm^2/g) across all glasses, irrespective of density or erbium oxide concentration. This outcome underlines that at higher γ-ray energy levels, the addition of Eu_2O_3 has negligible impact on the radiation competence properties of these blocks. In Fig. 5b, it's evident that both the Phys-X and XCOM methods yield identical results when assessing the MAC values for the BCBEu0.4 sample. Moreover, the outcomes directed to that the BCBEu1.0 block, containing the uppermost erbium oxide

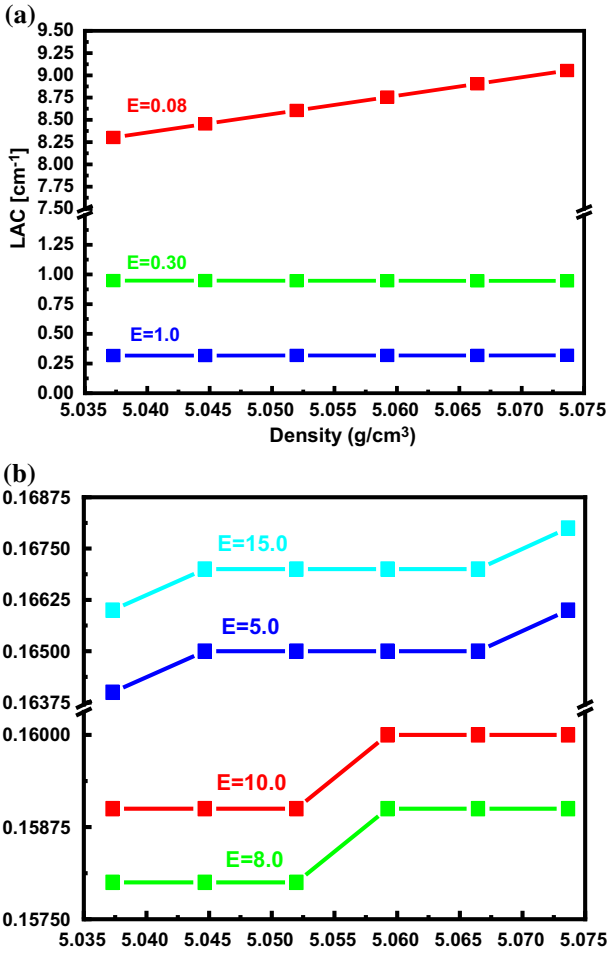

Fig. 7 LAC as a function of glass sample density for **a** E = 0.08, 0.3, and 1 MeV and **b** E = 5, 8, 10, and 15 MeV

concentration, exhibits the highest MAC within spectrum of energies examined in this study.

Figure 6a displays the functionality of LAC across the entire domain of incident energies for γ-rays as pointed our earlier. The photon energy of E = 15 keV, distinct values are observed: 204.650, 205.688, 206.721, 207.751, 208.776, and 209.796 cm^{-1}, corresponding respectively to BCBEu0.0–BCBEu1.0 samples. Their percentage ratio at higher and lower energies remains consistent with the MAC values, indicating their dependence on sample density. These outcomes suggest an influential relationship among the obtained values and the calculated V_m of the glass systems. The sample labeled as BCBEu1.0 exhibits the highest LAC values. Figure 6b presents a bar chart depicting the sample BCBEu1.0 having the maximum LAC value between the tested blocks. The chart demonstrates a rapid decrease in LAC values with respect to incoming photon energy.

The influence of sample density on linear mass attenuation coefficients are illustrated in Fig. 7a for E = 0.08, 0.3, and 1 MeV and Fig. 7b for 5, 8, 10, and 15 MeV. The figure reveals the following facts: at low energy (E = 80 keV), we find that $8.30 < LAC < 9.05$ cm^{-1}. In the middle energy range (e.g. around $E \approx 1.0$ MeV), LAC values sharply decline as low

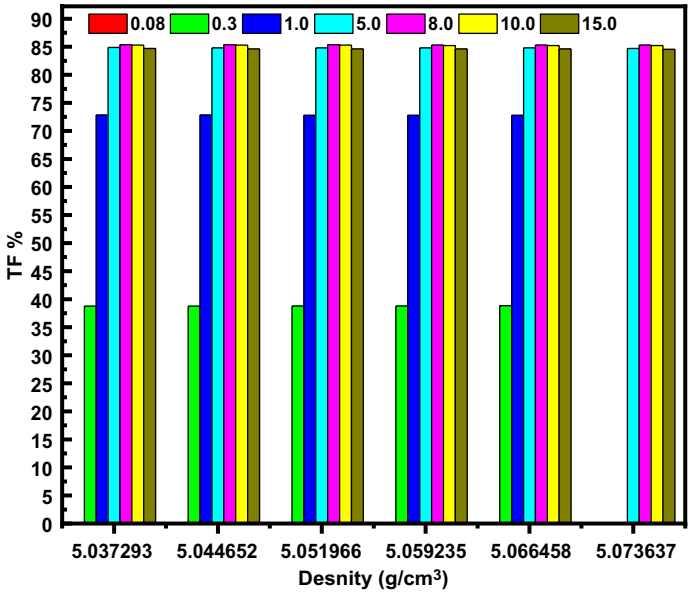

Fig. 8 TF of the incident gamma-ray photons at selected incoming photon energy indicated at the top of bars. The TF values are evaluated at sample's thickness x = 1.0 cm

as 0.32 cm^{-1}, and at higher-energies photons, they drop to around 0.17 cm^{-1}. However, the general trend of this parameter relative to density remains consistent, with an increasing trend as density increases.

Moreover, Fig. 8 displays the γ-rays TF% of the transparent blocks at various photons energies levels and at block width x = 10.0 mm. This figure highlights two key characteristics: low transmission for lower-energetic photon and leveling off at higher energy, sparking the essence of Beer–Lambert's model. Additionally, for a specific sample density, the transmission factor (TF) increases with photon energy, reaching a peak at E = 8.0 MeV before decreasing. This pattern also emphasizes the impact of block width on radiation attenuating performance of γ-rays as they interact with the medium. The figure underlines the dependency of TF% on sample's densities and gamma-ray energies, being higher for higher-energy and lower-density conditions. For instance, at a density = 5.059235 g/cm^3 (BCBEu0.6) and block width = 10.0 mm, TF values for indicated energies in the figure are 0.02%, 38.8%, 72.8%, 84.8%, 85.3%, 85.2%, and 84.6% respectively. Furthermore, additional analysis of shielding properties is performed to gain deeper insights into the interaction of Eu_2O_3 with gamma-ray radiation.

The HVL has been computed and juxtaposed with conventional glass references (designated as RS-360 and RS-520 (El-Mallawany et al. 2018)), as presented in Fig. 9a and b. Regarding E = 411 keV as in Fig. 9a, the HVL of the examined samples displays nearly no correlation with molar percentage, although their magnitudes exceed those of the RS-520 variant while being inferior to RS-360 (El-Mallawany et al. 2018). The HVL proportionality ratios between the ongoing specimen and the standard references stand at 0.81 and 1.5 for RS-520 and RS-360 correspondingly. In contrast, at E = 1010 keV, all specimens manifest almost identical HVL values, albeit lesser than the HVL magnitudes for RS-360 and RS-520 as shown in Fig. 9b. Figure 10 depicts the variation of the effective atomic number

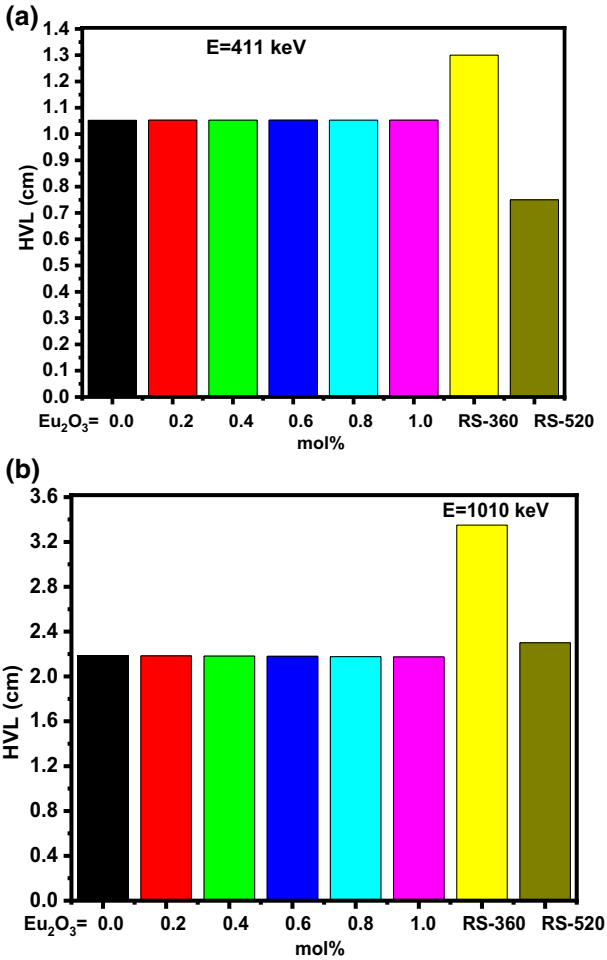

Fig. 9 A comparison between the HVL for the current investigated samples with other RS-360 and RS-520 standard glasses at **a** E = 411 keV and **b** E = 1010 keV

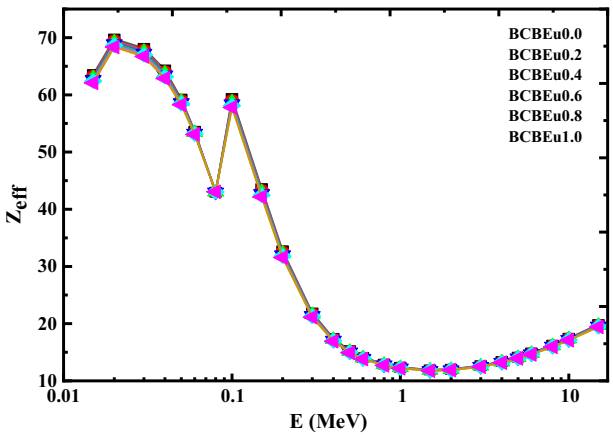

Fig. 10 Variation of Zeff as a function of photon energy (E) of the investigated samples

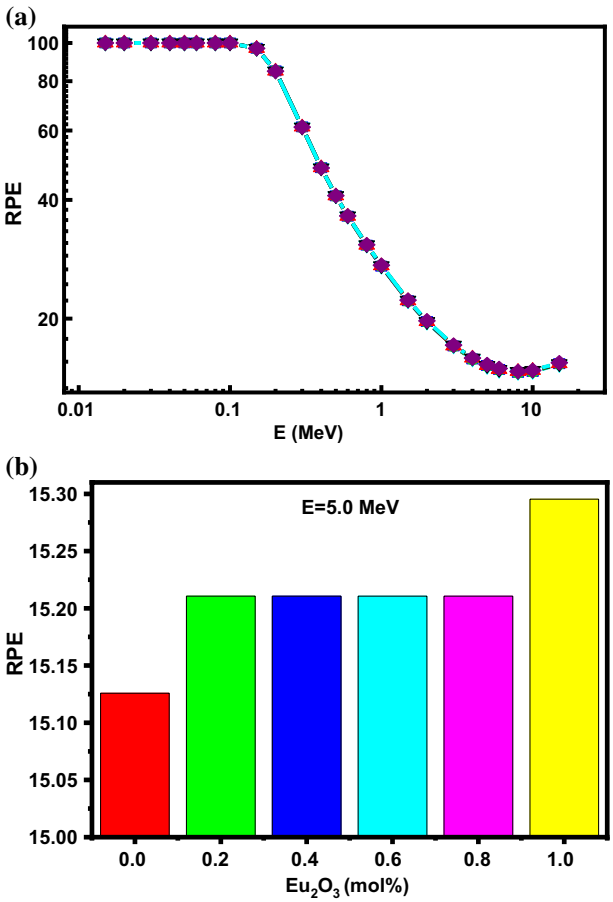

Fig. 11 **a** The RPE for the studied samples as a function of incident photon energy. **b** The RPE evaluated at E = 5.0 MeV

(Z_{eff}) parameter as a function of photon energy (E) of the investigated samples. As shown in Fig. 10, the trend of the Z_{eff} is the same of MAC trend.

The radiation safeguard efficacy, denoted as (RPE = 1-TF), is visualized in Fig. 11a. For low-energy domains, RPE approaches nearly 100% and gradually diminishes with the escalation photonic energies. The figure shows the RPE is the lowest for BCBEu0.0 (*i.e.*, least Eu^{3+}) sample and greatest for BCBEu1.0 (*i.e.*, greatest Eu^{3+}). The RPE is evaluated at sample thicknesses x = 1.0 cm. The diagram also portrays this metric at E = 5.0 MeV is shown in Fig. 11b. The specimen labeled BCBEu1.0 demonstrates superior RPE values across the entire energy spectrum, showcasing the marked influence of [Eu_2O_3] molar fraction. This deduction underscores that contingent on the scrutinized shielding attributes to density, molar fraction, OPD, or OMV of the investigated glasses. The pivotal determinant for optimal shielding pertains to the specific application context.

The graphical representation in Fig. 12 displays the effective fast-neutron-removal-cross-section (denoted as Σ_R and measured in cm^{-1}) for each sample using bar visualization. The computed Σ_R values for the glass samples reveal that BCBEu1.0 exhibits the

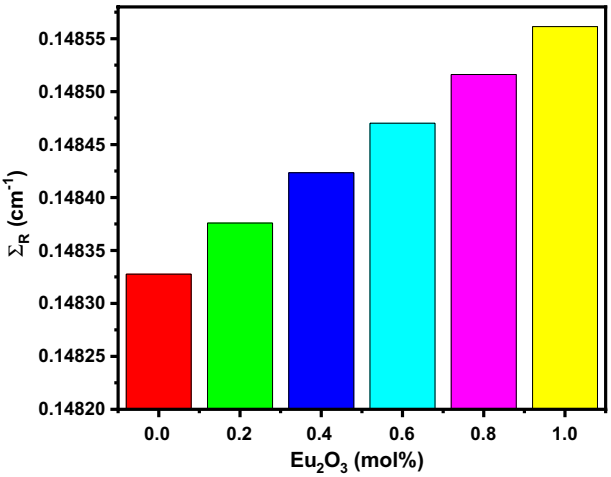

Fig. 12 The fast neutron effective removal cross section Σ_R for the studied samples. Sample BCBEu1.0 of the highest density has the dominant value among all glass samples

highest result ($\Sigma_R = 0.14856$ cm^{-1}). This particular sample possesses the greatest molar fraction of [Eu_2O_3] at 1.0 mol%, which corresponds to the highest molar volume but the lowest Vickers Hardness (recorded at 30.59 GPa, as indicated in Table 2). Conversely, the sample BCBEu0.0, which contains the lowest [Eu_2O_3] mol%, density, molar volume, OMV, and Vickers's Hardness (measured at 30.62 GPa), demonstrates the lowest computed Σ_R value of 0.14833 cm^{-1}. This sample also has the lowest molar volume and OPD among the other glass compositions studied. Figure 12 additionally illustrates a gradual increase in Σ_R that correlates with the observed patterns in molar volume and density (refer to Fig. 3). The interrelated fluctuations of Σ_R in relation to the physical–mechanical hallmarks suggest a prospective approach where the intended glasses compositions could potentially accommodate engineered and γ-rays defenses requirements within a specific application context (Wood 1982; Dong et al. 2017).

4 Conclusion

Six glass blocks of chemical composition $70B_2O_3$–20CaO–$(10-x)Bi_2O_3$–xEu_2O_3: 0 (BCBEu0.0) $0.0 \le x \le 1.0$ (BCBEu1.0) mol% has been set the traditional melt-quenched-method. Structure, physical, mechanical properties as well as gamma-ray shielding characteristics of these transparent blocks were investigated. XRD measurements proposed the glasses were in their amorphous state. Sample density (ρ_{glass}) found to be from 5.0373 to 5.0736 g/cm^3, while the V_m decreased from 25.012 to 24.605 cm^3/mol as a function of Eu_2O_3 molarity up to 1.0 mol%. OMV decreased from 9.62 cm^3/mol at [Eu_2O_3] = 0 mol% to 9.46346 cm^3/mol at [Eu_2O_3] = 1.0 mol% in the glass structure. Poisson's glasses ratio varies between 0.250 and 0.257. The Young's (E) modulus ranged between 63.202 and 65.002 GPa. The shielding efficiency reflected on MAC and LAC was found to increase as the mol% of Eu_2O_3. The glass BCBEu1.0 with high density found to have the lowest

values of HVL. The BCBEu1.0 block showed the optimum RPE% values, pinpointing to effluence of [Eu_2O_3] molar fraction. The BCBEu1.0 glass showed highest value of the $\Sigma_R = 0.14856\ cm^{-1}$. Results revealed that the proposed glass sample (BCBEu1.0) is considered a suitable material in field of medical application due to high ability for radiation protection and mechanical properties as compared to investigated samples. The future directions for research will use other rare earths and compare between them.

Acknowledgements The authors extend their appreciation to the Deputyship for Research & Innovation, Ministry of Education in Saudi Arabia for funding this research work through the project number RI-44-0086.

Author contributions NAMA, and YSR: wrote the main manuscript text; RAS, HA, EMM and YSR: prepared and drown all figures; all authors reviewed and revised the manuscript.

Funding The authors extend their appreciation to the Deputyship for Research & Innovation, Ministry of Education in Saudi Arabia for funding this research work through the project number RI-44-0086.

Availability of data and materials All data generated or analyzed during this study are included in this published article.

Declarations

Conflict of interest The authors declare that they have no conflict of interest.

Consent to participate Not applicable.

Consent to publish Not applicable.

Ethical approval Authors declare that this manuscript is original, has not been published before, and is not currently being considered for publication elsewhere.

References

Abdel Maksoud, M.I.A., Sallam, O.I., Kassem, S.M., Fahim, R.A., Awed, A.S.: Novel strategy for hazardous cement bypass dust removal: structural, optical and nuclear radiation shielding properties of CBD-bismuth borate glass. J. Inorg. Organomet. Polym. Mater.. Inorg. Organomet. Polym. Mater. **32**, 3533–3545 (2022)

Adam, J.L.: Lanthanides in non-oxide glasses. Chem. Rev. **102**, 2461–2476 (2002)

Alsaif, N.A.M., Elsad, R.A., Abdel-Aziz, A.M., Ahmed, E.M., Rammah, Y.S., Misbah, M.H., Shams, M.S.: Linear optical characteristics as well as gamma-ray shielding capabilities of quaternary lithium-zinc borate glasses with Y^{3+} ions. Opt. Mater. **131**, 112673–112680 (2022a)

Alsaif, N.A., Elsad, R.A., Sadeq, M.S., Rammah, Y.S., Ahmed, E.M., El-Hamalawy, A.A., Shams, M.S.: Antimony (III) oxide-reinforced lithium-calcium borate glasses: preparation and characterization of physical, optical, and γ-ray shielding behavior through experimental and theoretical methods. J. Mater. Sci. Mater. Electron. **51**, 5869–5879 (2022b)

Babu, S.S., Babu, P., Jayasankar, C., Sievers, W., Tröster, T., Wortmann, G.: Optical absorption and photoluminescence studies of Eu^{3+}-doped phosphate and fluorophosphate glasses. J. Lumin. **126**, 109–120 (2007)

Berger, M.J., Hubbell, J.H.: XCOM: Photon Cross-Sections Database, Web Version 1.2 (n.d.)

Bray, P.J.: NMR and NQR studies of boron in vitreous and crystalline borates. Inorg. Chim. Acta **289**, 158–173 (1999)

Divina, R., Naseer, K.A., Marimuthu, K., Alajerami, Y.S.M., Al-Buriahi, M.S.: Effect of different modifier oxides on the synthesis, structural, optical, and gamma/beta shielding properties of bismuth lead borate glasses doped with europium. J. Mater. Sci. Mater. Electron. **31**, 21486–21501 (2020)

Dong, M.G., Sayyed, M.I., Lakshminarayana, G., Çelikbilek Ersundu, M., Ersundu, A.E., Nayar, P., Mahdi, M.A.: Investigation of gamma radiation shielding properties of lithium zinc bismuth borate glasses using XCOM program and MCNP5 code. J. Non-Cryst. **468**, 12–16 (2017)

El-Denglawey, A., Zakaly, H.M.H., Alshammari, K., Issa, S.A.M., Tekin, H.O., AbuShanab, W.S., Saddeek, Y.B.: Prediction of mechanical and radiation parameters of glasses with high Bi_2O_3 concentration. Results Phys. **21**, 103839–103848 (2021)

El-Mallawany, R., Sayyed, M.I., Dong, M.G., Rammah, Y.S.: Simulation of radiation shielding properties of glasses contain PbO. Radiat. Phys. Chem. **151**, 239–252 (2018)

Elsad, R.A., Abdel-Aziz, A.M., Ahmed, E.M., Rammah, Y.S., El-Agawany, F.I., Shams, M.S.: FT-IR, ultrasonic and dielectric characteristics of neodymium (III)/ erbium (III) lead-borate glasses: experimental studies. J. Mater. Res. Technol. **13**, 1363–1373 (2021a)

Elsad, R.A., Rammah, Y.S., El-Agawany, F.I., Ahmed, E.M., Shams, M.S.: Er^{3+}/Nd^{3+} ions reinforced lead-borate glasses: an extensive investigation of physical, linear optical characteristics, and photon shielding capacity. J. Mater. Res. Technol. **14**, 3161–3170 (2021b)

Hegde, V., Kamath, S.D., Kebaili, I., Sayyed, M.I., Sathish, K.N., Viswanath, C.S.D., Pramod, A.G., Ramesh, P., Keshavamurthy, K., Devarajulu, G., Jagannath, G.: Photoluminescence, nonlinear optical and gamma radiation shielding properties of high concentration of Eu_2O_3 doped heavy metal borate glasses. Optik **251**, 168433–168445 (2022)

Khan, I., Rooh, G., Rajaramakrishna, R., Sirsittapokakun, N., Kim, H., Kaewkhao, J., Kirdsiri, K.: Energy transfer phenomenon of Gd^{3+} to excited ground state of Eu^{3+} ions in Li_2O–BaO–Gd_2O_3–SiO_2–Eu_2O_3 glasses. Spectrochim. Acta A Mol. Biomol. Spectrosc. **210**, 21–29 (2019)

Khattari, Z.Y., Alsaif, N.A., Rammah, Y.S., Abou Hussein, E.M., Shams, M.S., Elsad, R.A.: Fabrication, physical, mechanical, and radiation protection properties of bismo-borate glasses containing La^{3+}+ Eu^{3+} as additive ions. Radiat. Phys. Chem. **201**, 110454–110462 (2022)

Lavın, V., Rodrıguez-Mendoza, U., Martın, I., Rodrıguez, V.: Optical spectroscopy analysis of the Eu^{3+} ions local structure in calcium diborate glasses. J. Non-Cryst. **319**, 200–216 (2003)

Madbouly, A.M., Sallam, O.I., Issa, S.A.M., Rashad, M., Hamdy, A., Tekin, H.O., Zakaly, H.M.H.: Experimental and FLUKA evaluation on structure and optical properties and γ-radiation shielding capacity of bismuth borophosphate glasses. Prog. Nucl. Energy **148**, 104219–104226 (2022)

Makishima, A., Mackenzie, J.D.: "Calculation of bulk modulus, shear modulus and Poisson's ratio of glass. J. Non-Cryst. **17**, 147–157 (1975)

Michaelis, V.K., Aguiar, P.M., Kroeker, S.: Probing alkali coordination environments in alkali borate glasses by multinuclear magnetic resonance. J. Non-Cryst. **353**, 2582–2590 (2007)

Niraula, B.B., Rizal, C.: Photoluminescence property of Eu^{3+} doped $CaSiO_3$ nano-phosphor with controlled grain size. Colloids Interfaces **2**, 52–64 (2018)

Poort, S., Reijnhoudt, H., Van der Kuip, H., Blasse, G.: Luminescence of Eu^{2+} in silicate host lattices with alkaline earth ions in a row. J. Alloys Compd. **241**, 75–81 (1996)

Rammah, Y.S., Mahmoud, K.A., Kavaz, E., Kumar, A., El-Agawany, I.: The role of PbO/Bi_2O_3 insertion on the shielding characteristics of novel borate glasses. Ceram. Int. **46**, 23357–23368 (2020)

Rammah, Y.S., El-Agawany, F.I., Gamal, A., Olarinoye, I.O., Ahmed, E.M., Abouhaswa, A.S.: Responsibility of Bi_2O_3 content in photon, alpha, proton, fast and thermal neutron shielding capacity and elastic moduli of $ZnO/B_2O_3/Bi_2O_3$ glasses. J. Inorg. Organomet. Polym. **31**, 3505–3524 (2021a). https://doi.org/10.1007/s10904-021-01976-5

Rammah, Y.S., Sayyed, M.I., El-bashir, B.O., Asiri, S.M., Al-Hadeethi, Y.: Linear optical features and radiation shielding competence of ZnO–B_2O_3–TeO_2–Eu_2O_3 glasses: Role of Eu^{3+} ions. Opt. Mater. **111**, 110525–110533 (2021b). https://doi.org/10.1016/j.optmat.2020.110525

Şakar, E., Özpolat, Ö.F., Alım, B., Sayyed, M.I., Kurudirek, M.: Phy-X/PSD: Development of a user friendly online software for calculation of parameters relevant to radiation shielding and dosimetry. Radiat. Phys. Chem. **166**, 108496–108507 (2020)

Sallam, O.I., Madbouly, A.M., Elalaily, N.A., Ezz-Eldin, F.M.: Physical properties and radiation shielding parameters of bismuth borate glasses doped transition metals. J. Alloys Compd. **843**, 156056–156065 (2020)

To, T., Jensen, L.R., Smedsjkaer, M.M.: On the relation between fracture toughness and crack resistance in oxide glasses. J. Non-Cryst. Solids **534**, 119946–119951 (2020)

Wagh, A., Raviprakash, Y., Kamath, S.D.: Gamma rays interactions with Eu_2O_3 doped lead fluoroborate glasses. J. Alloys Compd. **695**, 2781–2798 (2017)

Wood, J.: Computational Methods in Reactor Shielding. Pergamon Press, Inc., New York (1982)

Yiannopoulos, Y., Chryssikos, G.D., Kamitsos, E.: Structure and properties of alkaline earth borate glasses. Phys. Chem. Glasses **42**, 164–172 (2001)

Authors and Affiliations

Norah A. M. Alsaif[1] · Haifa I. Alrebdi[1] · Y. S. Rammah[2] · R. A. Elsad[3] · E. M. Mounir[1]

✉ Y. S. Rammah
dr_yasser1974@yahoo.com

Norah A. M. Alsaif
noaalsaif@pnu.edu.sa

Haifa I. Alrebdi
hialrebdi@pnu.edu.sa

R. A. Elsad
ragab.elsad@gmail.com

E. M. Mounir
emmohammed@pnu.edu.sa

[1] Department of Physics, College of Science, Princess Nourah Bint Abdulrahman University, P.O. Box 84428, 11671 Riyadh, Saudi Arabia

[2] Department of Physics, Faculty of Science, Menoufia University, Shebin El-Koom 32511, Egypt

[3] Basic Engineering Science Department, Faculty of Engineering, Menoufia University, Shebin El-Koom 32511, Egypt